AT&T BELL LABORATORIES TECHNICAL JOURNAL
Vol. 63, No. 2, February 1984
Printed in U.S.A.

Experimental Ion-Implanted Bubble Memory Device With 16-μm^2 Cell

By T. J. NELSON,* D. J. MUEHLNER,* V. V. S. RANA,* B. J. ROMAN,* and G. P. VELLA-COLEIRO*

(Manuscript received April 1, 1983)

This paper describes a 4-μm-period (16 μm^2/bit) magnetic bubble device based on ion-implanted propagation patterns. Single-layer LaSmLuBiGa–IG films were implanted with Ne^+ and He^+ ions using densified photoresist masking patterns. Coarse (three eighths of a period) minimum features were used in the Permalloy and Al-Cu levels. A 21-Oe overlap bias range was obtained for generation, propagation, transfer, and detection at 55-Oe drive. Generation and detection were demonstrated to have a 39-Oe bias range at 44-Oe drive, and a 39-Oe bias range for minor-loop propagation was obtained at $\geq$33-Oe drive.

I. INTRODUCTION

Using proposed scaling laws for Permalloy†-based magnetic bubble devices, Kyrder[1] has concluded that 6×10^6 b/cm^2, 1-μm bubble devices should be achievable. Fontanta et al.[2] have studied devices using 4.75 $\times$ 5.25-μm^2 cells and 0.75-μm gaps fabricated with 10X reduction, direct step on wafer projection printing. Quasistatic gate operation was achieved at 70-Oe drive field. Recently, Yanase et al.[3] demonstrated propagation on 4-μm "club foot" circuits with 1-μm gaps at

* AT&T Bell Laboratories.

† Permalloy is a trademark of the Allegheny Ludlum Steel Corporation.

drive fields above 45 Oe. It appears, therefore, that Permalloy-based bubble devices are already near their anticipated density limit.

One-micrometer bubble devices with 30-μm^2 cell area have been operated[4] at 150 kHz, using Ion-Implanted Propagation Patterns[5] (I2P2s) instead of Permalloy. And Komenou et al.[6] have reported promising results using 16-μm^2 I2P2 cells. Because of their extreme simplicity (a sine-wave-shaped track will propagate, for example), I2P2 devices can be resolved with three-eighths of a period minimum features, which, together with a 0.75-μm optical lithography limit, imply a possible density of $2.5(10)^7$ b/cm^2.

This paper describes magnetic bubble material and test-circuit design and characterizes generation, propagation, transfer, and detection in 4-μm-period devices based on ion-implanted propagation patterns (see Fig. 1).* With one exception, the minimum features in the Permalloy and Al-Cu levels were coarsened to three-eighths of a period. We have continued to use single-layer garnet films, and the layers processed on the chip were unchanged, except that the Permalloy thickness was reduced from 500 AU to 375 AU.

II. MATERIAL FOR 4-μm-PERIOD BUBBLE DEVICES

Films of the nominal composition $(LaSmLu)_3(FeGa)_5O_{12}$, with and without Bi, were used in the present study. Propagation at 4-μm period in films of $(LaSmLuCa)_3$ $(FeGe)_5O_{12}$ composition was previously reported.[7] However, this composition required a high magnetic moment ($4\pi M_s$ = 784G) to produce 1.1-μm-sized bubbles. The saturation magnetization ($4\pi M_s$) is given by $4\pi M_s = \sqrt{32\pi AQ/\ell^2}$, where ℓ is the material length parameter, Q is the quality factor, and A is the exchange constant. Hence, a similar bubble size (same ℓ, and Q) can be obtained at a lower $4\pi M_s$ by going to a composition having a lower exchange constant. Since A scales with the Curie temperature,[7] the required $4\pi M_s$ can be lowered by going to a composition having a lower Curie temperature. In the present work we have used Ga substitution, instead of CaGe, to reduce the $4\pi M_s$ and, possibly, the minimum drive field. The desired anisotropy was obtained from the SmLu site selectively. The bubble mobility was improved by making use of the Lanthanum effect;[7,8] i.e., the Sm content was kept low and the uniaxial anisotropy was increased by increasing the Lu content and using La to match the film lattice parameter to that of the substrate, La having no effect on the uniaxial anisotropy.

---

* The contents of this paper were presented by T. J. Nelson in the Fourth International Conference on Magnetic Bubbles held September 24–27, 1980, in Tokyo.

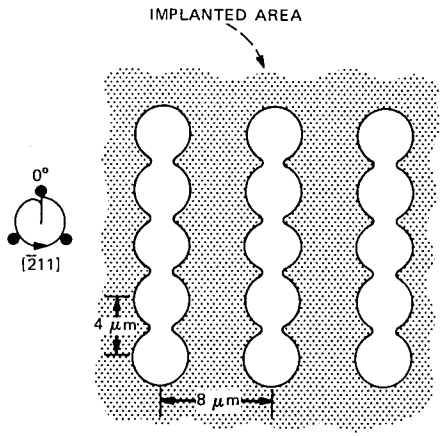

Fig. 1—Minor-loop ion-implanted propagation patterns and orientation with respect to wafer, preferred positions, and rotating field conventions.

Films were grown from $PbO—B_2O_3$ flux by the Liquid Phase Epitaxy (LPE) technique on 50-mm diameter (111) $Gd_3Ga_5O_{12}$ substrates by horizontal dipping with a unidirectional rotation of 100 rpm. The growth temperatures ranged from 872° to 880°C. Table I lists the properties of typical films. The film thickness and demagnetized stripe width intentionally exceed the 0.9 μm desired for 4-μm period to allow for the thickness of the implant. H_o is the collapse field. The domain wall mobility (μ) was calculated from the resonance line width using standard Ferromagnetic Resonance (FMR) technique. Initially, films were grown without bismuth (type A). The bubble visibility in these films was poor because of the low Faraday rotation (θ_F). The addition of Bi was made (film type B) to produce an enhanced (and reversed) Faraday rotation to improve the bubble visibility.

The anisotropy of the implanted films was determined from microwave resonance using the method described in Ref. 9. Measurements were made at 11.85 GHz on 50-mm diameter wafers after removing the film on the back side by etching in phosphoric/sulfuric acid. Figure 2 shows the derivative microwave absorption vs. field of a film (type A). This film was implanted with 80/Ne/1E14, 270/Ne/2E14, and 130/He/6E15 followed by a 300°C anneal. (The implantations are referred to in a shorthand form representing energy in keV/ion species/dose in ions/cm^2.) The anisotropy fields of both the film and its implant can be read from Fig. 2. For this film,

$$Q = 1 + \frac{770}{664} = 2.16.$$

A sufficiently large change in anisotropy of about 6(10)^4 ergs/cm^3 was

Table I—Properties of $(LaSmLu)_3(FeGa)_5O_{12}$ films

		Property							
	Type	th (μm)	sw (μm)	ℓ (μm)	H_o (Oe)	$4\pi M_s$ (G)	H_K (Oe)	μ (cm/s/Oe)	θ_F (at 5000Å) (degrees/cm)
A	Without Bi	1.39	1.08	0.11	378	664	1435	485	1400
B	With Bi	1.22	1.07	0.11	365	655	1650	400	−4500

caused by the implantation. Figure 3 shows the visually obtained minor-loop bias margins vs. drive field on another film (type B). This film was implanted with 80/Ne/1E14 (no pattern) and 270/Ne/2E14 + 130/He/4E15 patterned implants. This sample was subjected to full processing, which included vacuum anneal at about 350°C for 1 hour prior to the Permalloy evaporation. The demagnetized strip width in the implanted region after processing was 0.85 μm, sufficiently close to the desired value.

III. PROCESSING OF 4-μm-PERIOD BUBBLE DEVICES

This study employed contact printing using chrome masters on glass. The test devices were originally encoded with 0.5-μm address steps at 8-μm period. For this study they were shrunk to 0.25-μm steps at 4-μm period using an Electron Beam Exposure System (EBES)[10] option. Scanning Electron Microscope (SEM) photographs of the propagate patterns are shown in Fig. 4a as printed in AZ1350J photoresist in the ordinary way and Fig. 4b as transferred to densified AZ1350J by trilevel[11] method. The latter lithographic technique permits the transfer of a high-resolution image, which is more easily achieved in a thin resist layer, into a thick polymerized layer that is dimensionally stable under extreme implantation conditions. Plasma-deposited SiO_2 separates the thin and thick organic layers and, after plasma etching through the primary resist pattern, serves as a reactive ion-etch mask to complete the image transfer process. Because of the highly anisotropic etching, trilevel patterns have vertical edge profiles and were used exclusively to guarantee edge integrity for the implanted patterns in this study.

The processing after implantation consisted of 2000 AU of plasma-deposited SiO_2 (P-SiO_2), 375 AU of Permalloy, and an additional 2000 AU of P-SiO_2 and 5000 AU of Al-Cu. Via holes were plasma etched into the second SiO_2 layer to connect the Permalloy sensors to their Al-Cu pads. The devices received no additional passivation. The Permalloy and Al-Cu layers were patterned with contact printing and ion-beam milling. As will be discussed below, the minimum features in the metal layers, except in the generator, were coded to be 1.5 μm.

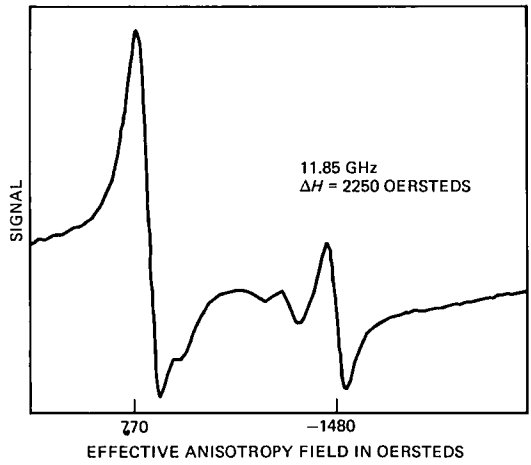

Fig. 2—FMR absorption (derivative) as a function of field of a $(LaSmLu)_3(GaFe)_5O_{12}$ film implanted with 80/Ne/1E14, 270/Ne/2E14, and 130/He/6E15.

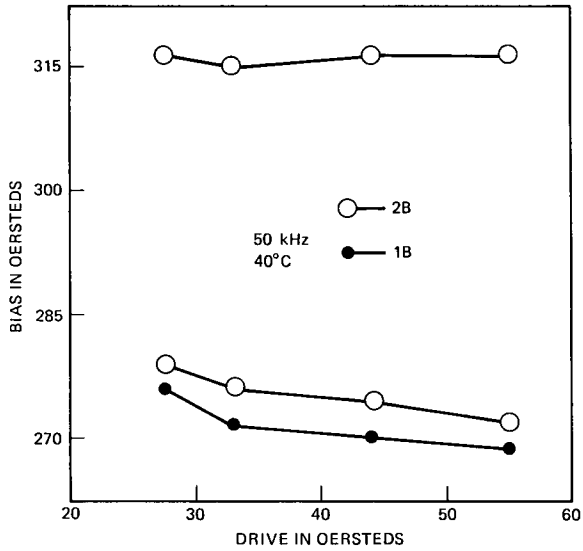

Fig. 3—Minor-loop propagation margins vs. drive field at 40°C using 80/Ne/1E14 (unpatterned) + 270/Ne/2E14 + 130/He/4E15. Open circles refer to two bubbles in adjacent positions.

IV. LAYOUT AND OPERATION OF 4-μ-PERIOD BUBBLE DEVICE

Figure 5 shows the components and layout used in this study. The generator consists of a simple Al-Cu hairpin, much like that used in Permalloy devices. Between the generator and detector, a line of clover-leaf-shaped features was interpolated. These features were sep-

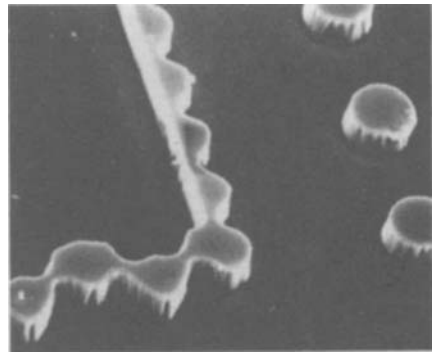

(a)

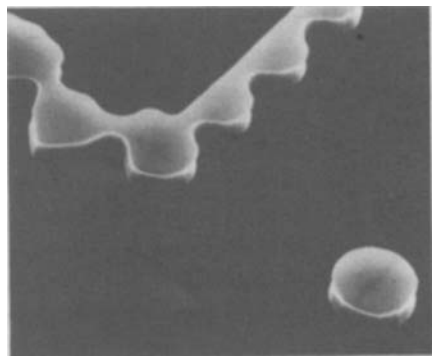

(b)

Fig. 4—SEM photographs of 4-μm-period resist patterns (a) with contact-printed AZ1350J resist and (b) using trilevel resist.

arated by 1-μm merge gaps.[12] The clover-leaf features have threefold symmetry, except for small EBES address effects, and so provide strong-side propagation all around. The transfer-enable was designed to frustrate propagation of bubbles by the merge gap and send them through the gaps and around the cover-leaf features. In this way, a block of bubbles coming from the generator may, when properly positioned, be brought to the transfer ports for insertion into the minor loops. The trapping-transfer gates[13] operate by confining bubbles within the lower slot of the conductor and between the two implant boundaries. Bubbles transfer from one path to the other after being trapped for approximately 180° of field rotation. When a group of bubbles is transferred out from the minor loops to the tops of the clover-leaf features, each bubble propagates around through the merge gap to the path between the generator and detector. Once the block is thus assembled, the bubbles propagate towards the detector with the same bit order as originally generated. The detector consists of an Al-Cu conductor hairpin to stretch the bubbles and a Permalloy stripe to

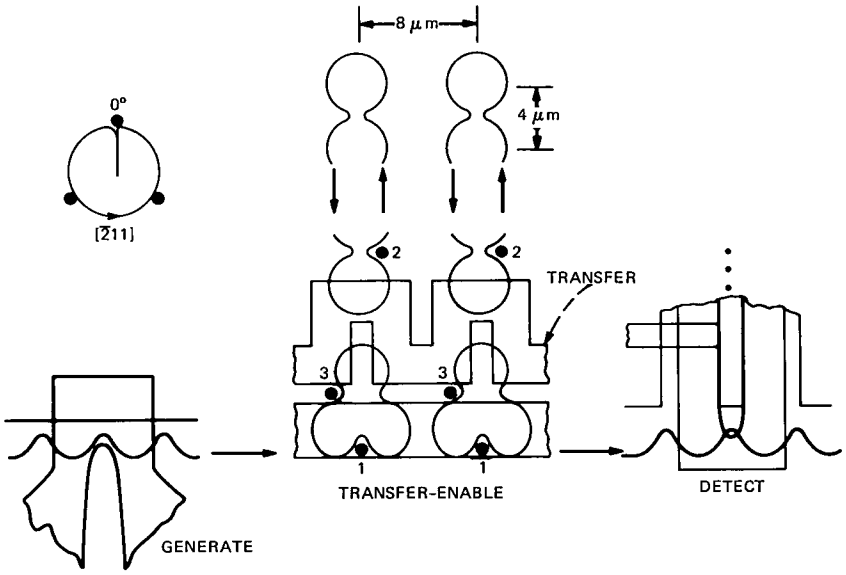

Fig. 5—Test-circuit layout used in design study at 4-μm period. Minimum feature was 1 μm in the implant level and 1.5 μm in the Permalloy and Al-Cu levels.

sense them. The bubbles are collapsed by a second current pulse to restore the detector for the next bubble.

The minimum coded feature used in the implant level was 1 μm, which was the distance between implanted regions through the narrowest place on the minor loops or the width of the implanted region in the gaps between clover-leaf features. Except for the generator, the minimum feature in the metal levels was coded to be 1.5 μm, which was the line width of the Permalloy sensor and the gap width in the Al-Cu hairpins. The Al-Cu line width in the transfer gates was made 2.5 μm, which is the maximum permitted by the 8-μm interloop spacing and the 1.5-μm gap width.

The experimental 4-μm-period devices (film type B) were operated on a microscope-based test set under microprocessor control. The temperature of the chips was unregulated, but as the duty factor for the drive coils was small and the bias magnet was water cooled, it was less than 25°C. All testing was carried out at 50 kHz with sine-wave currents in the drive coils. Figure 5 shows positions 1 through 3 where bubbles were stopped during the tests. A typical test consisted of (1) generation and propagation to 1; (2) propagation with transfer-enable and transfer-in to 2; (3) propagation around the minor loop back to 2; (4) propagation and transfer-out to 3; and, finally, (5) propagation and detection. The test was automatically repeated at 3-Oe bias intervals. The data pattern generated was compared with that actually detected,

and the exclusive OR of the two was printed for each test. The bias ranging could be restricted to a single component of the test, in which case the other components were performed at a fixed bias. All current pulsers were triggered at 0° in the appropriate cycles by the computer, and delays, widths, and amplitudes were manually adjusted on the pulsers.

V. DEVICE COMPONENTS AT 4-μm PERIOD

5.1 Generation

The generator design, shown in more detail in Fig. 6, was included in a serial test circuit also present on the chip. Ordinary ungapped propagation patterns were employed in the serial test circuit, which was used to obtain the generator and detector data given in Figs. 7, 9, and 10. A reduction in upper bias margin with increased pulse width was observed. At 100-ns pulse width, the full bias range was obtained with generator current varied almost by a factor of 2, from 110 to 200 mA.

5.2 Detection

Figure 8 shows the detector design employed. The Al-Cu hairpin was pulsed to remove the bubble from the strong-side track and simultaneously stretch it along the Permalloy at a drive-field angle of 90°. At this time the magnetization in the Permalloy switches from up to down. A decreased resistance is observed when a stripped-out bubble is present, indicating increased cross-magnetization. Figure 9 shows the stretch-current amplitude dependence of the bias margins for the approximately 50-μm-long detector in the serial test circuit. Good bias margins were obtained between 50 mA and 90 mA. Figure

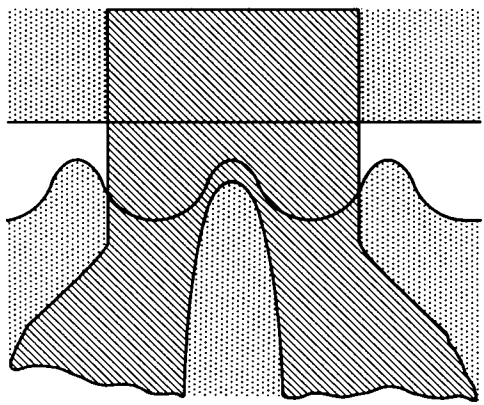

Fig. 6—Generator design using 1.5-μm slot width and 2.5-μm line width in the Al-Cu level.

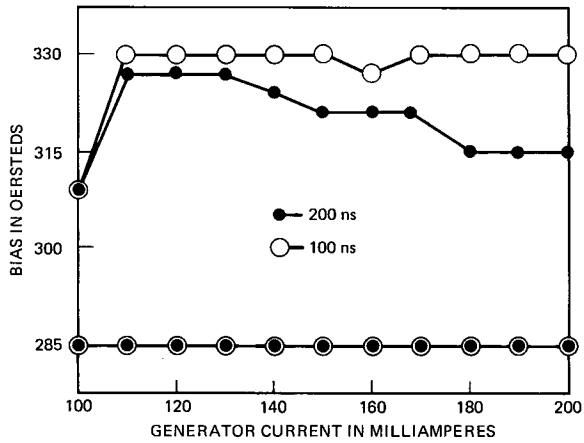

Fig. 7—Bias range at 55-Oe drive and 25°C for generation at 0° as a function of current.

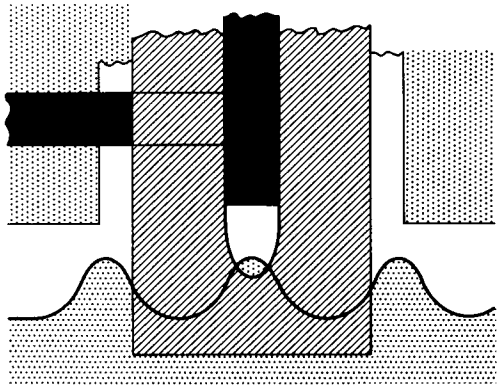

Fig. 8—Destructive Read Out detector design using 1.5-μm Permalloy line width and 2.5-μm Al-Cu line width at 4-μm period.

10 shows the bias-range dependence on collapse current amplitude. The collapse pulse was applied typically quite late, which stroboscopic observation (at 8-μm period) suggests gives the strip time to contract to a bubble before the collapse pulse is applied. Therefore, the collapse pulse is thought to collapse only a bubble, not a strip. Figure 11 shows the bias range vs. drive field for generation, strong-side propagation and detection. The bias range has opened up at 44-Oe drive, though operation was possible down to 33 Oe with some loss of low bias margin. The data presented in Figs. 7, 9, and 10 were taken at 55-Oe drive to be compatible with the transfer results given below.

Figure 12 shows the differential voltage between detector and

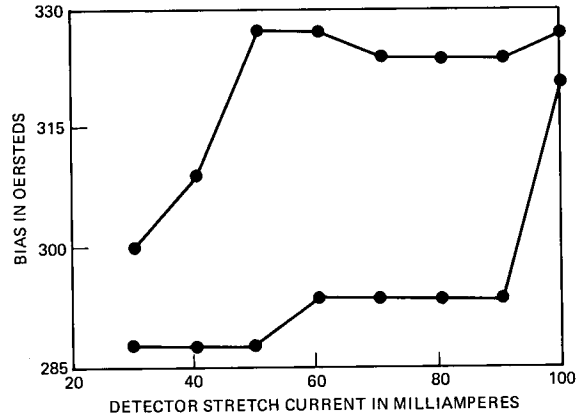

Fig. 9—Bias range vs. detector stretch current at 55-Oe drive field with pulse active between 72° and 126°.

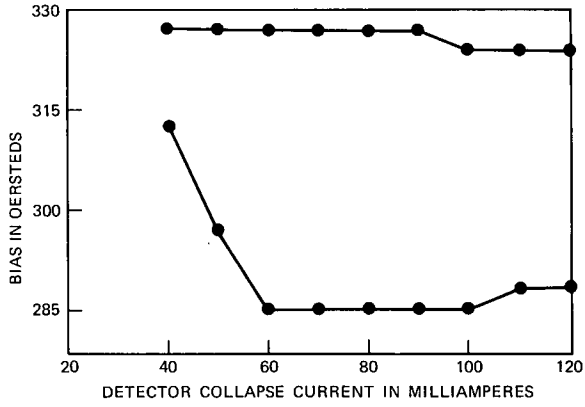

Fig. 10—Bias range vs. collapse pulse current at 55-Oe drive field with pulse timing 252° to 288°.

dummy, amplified by 10. This waveform was obtained at 55-Oe drive with the circuit for which transfer and minor-loop margins are given below. Reliable detection with this longer (100 μm compared to 50 μm in the serial test circuit) detector required earlier phasing for the stretch pulse, about 54° instead of 72°. In this particular circuit a higher collapse current was also needed. The 500Ω detector gave about 6 mV at 2.5 mA, corresponding to a figure of merit of $\delta V/V \approx 0.5$ percent.

5.3 Transfer-enable

The transfer-enable and trapping-transfer ports are drawn to larger scale in Fig. 13. The major line is composed of the bottoms of the

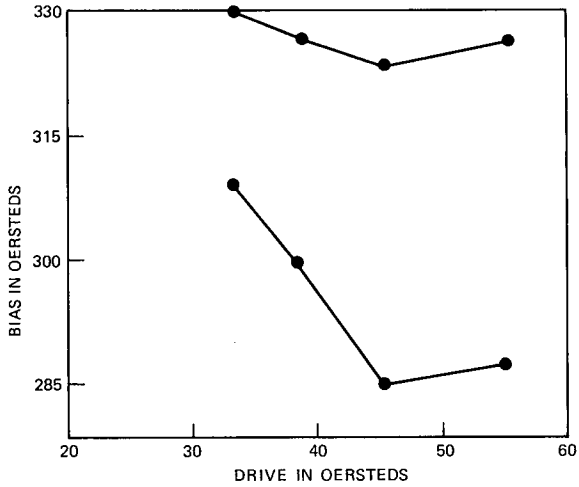

Fig. 11—Bias range for generation, strong-side propagation, and detection at 25°C vs. drive field.

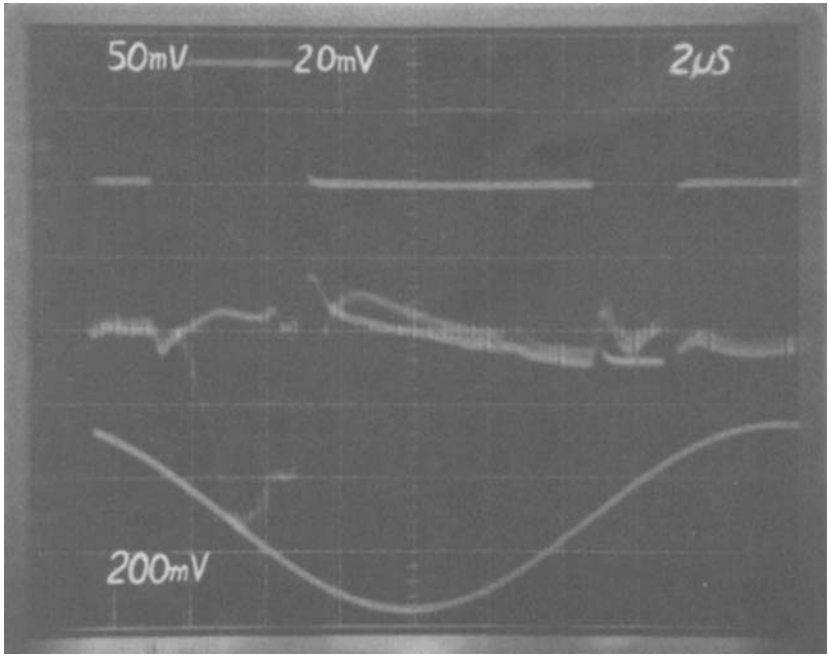

Fig. 12—Differential detector output with bubble and no bubble traces superimposed. Gain is 10 for the signal and 1 mV/mA for the stretch and collapse pulses. Positive peak of the sine wave is at 0°.

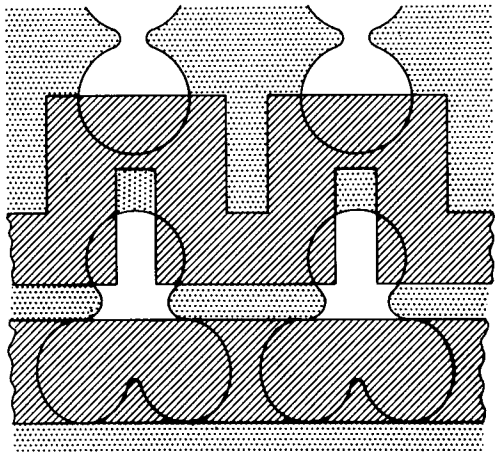

Fig. 13—Transfer-enable and trapping-transfer designs used to communicate between minor loops and gapped major line.

clover-leaf features. While bubbles propagated past the gaps at lower drive, at least 50 Oe was needed to propagate bubbles away from the clover-leaf cusps. The data reported below were obtained with 55-Oe sine-wave drive. Transfer-enable bias range vs. pulse current is shown in Fig. 14. Four bubbles, aligned with four ports, were made to pass through the merge gaps by a pulse active near a rotating field phase of 0°. The bubbles started from the cusps on the major line, passed through the gaps at the end of the first cycle, and propagated three steps around the clover leaf. A 33-Oe bias range was obtained for 25 through 45 mA pulses active from −72° to 36°. Some variation has been seen with other chips of the same wafer. In other tests, for example, the low bias limit increased with increasing current instead of being independent of current as in Fig. 14.

5.4 Trapping transfer

Figure 13 also shows trapping-transfer gates linking the tops of the clover-leaf features with the bottoms of the minor loops. For the data presented in Figs. 15 through 20, a single bubble was loaded into each of three adjacent 73-step minor loops. Note that the trapping-transfer conductor slot opens away from the minor loops. This means that the pulse increases the bias on neighboring positions in the minor loops. In this work, the effect of the pulse current on neighboring positions was investigated by pulsing one cycle before and one cycle after the bubbles propagated by the gates within the minor loops. The open circles in Figs. 15 through 20 represent, with these extra pulses, both transfer-in and transfer-out. The slot orientation was chosen to avoid

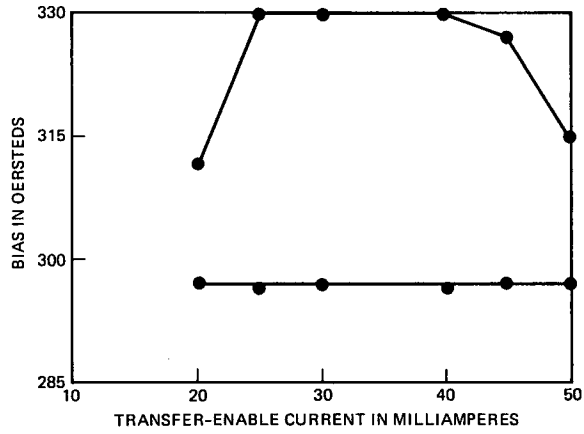

Fig. 14—Bias range vs. transfer-enable current at 55-Oe drive with pulse active from −72° to 36°.

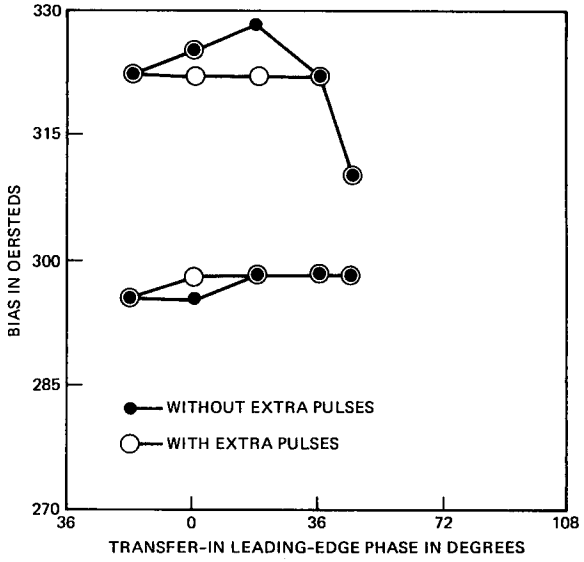

Fig. 15—Bias range vs. transfer-in leading-edge phase at 55 Oe. Trailing edge was held constant at 144° and the current was 35 mA.

the bad conductor crossings that developed after passivation in 8-μm trapping-transfer gates. In the present design, the bad crossing would be expected if the conductor slot extended past the implant boundary of the bottom of the minor loop. In the 8-μm-period gates, the crossings were still good after passivation when the slot stopped short, as in Fig. 13, and left continuous metal over the bubble path.

Figure 15 shows bias range vs. leading-edge phase of the transfer-in pulse. The pulse could be started as late as +36°; thereafter, the upper bias margin dropped abruptly. The bias range was fairly constant for earlier phases. Transfer-in trailing-edge phase was varied to produce Fig. 16. Figure 17 shows the bias range vs. transfer-in current, with the lowest current for reliable operation at 30 mA. The high bias effect of the pulse on neighboring positions in the minor loop was most noticeable in this plot. The overall margins were limited by transfer-in at low bias, which improved as the current was lowered. Figure 18 shows the bias range vs. transfer-out leading-edge phase. Figure 19 shows that a higher upper bias limit exists for trailing-edge phases near 360°. Such phasing, however, loses high bias margin when the effect on bubbles in adjacent cycles is considered. This high bias failure mode is also clearly evident in Fig. 20, which shows the bias range vs. transfer-out current. The overall margins were in fact limited at high bias by transfer-out.

VI. OVERALL BIAS RANGE AND CONCLUSIONS

Figure 21 shows the bias ranges for individual device components at 55-Oe drive. These results were obtained with the chip also used to produce the data shown in Figs. 14 through 20. The enable, transfer, and detector designs have been discussed above. The generator in the major-minor test circuit had 1-μm gap and 1.75-μm coded line widths.

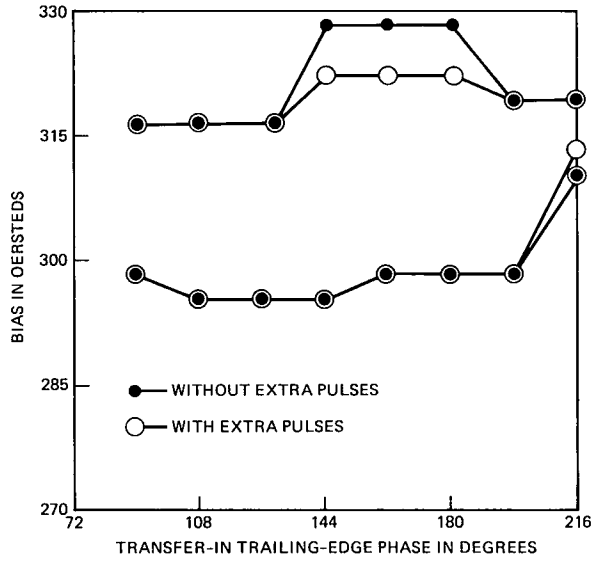

Fig. 16—Bias range vs. transfer-in trailing-edge phase at 55 Oe with leading edge at 0° and the current at 35 mA.

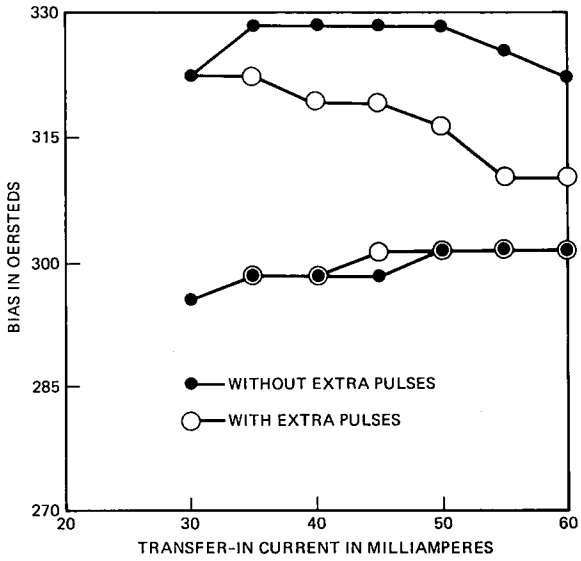

Fig. 17—Bias range vs. transfer-in current at 55 Oe with pulse active from 0° to 144°.

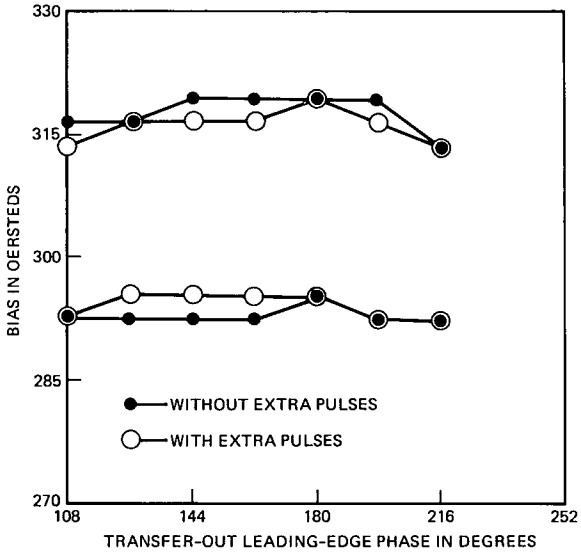

Fig. 18—Bias range vs. transfer-out leading-edge phase at 55 Oe. Pulse current was 45 mA and lasted until 306°.

In other work we have found 1.5-μm gaps to be satisfactory for generation at 4-μm period. A generator pulse of 105 mA, lasting 80 ns, worked well on the chip of Figs. 14 through 21. In other nominally identical chips, higher currents, over 200 mA, were required for gen-

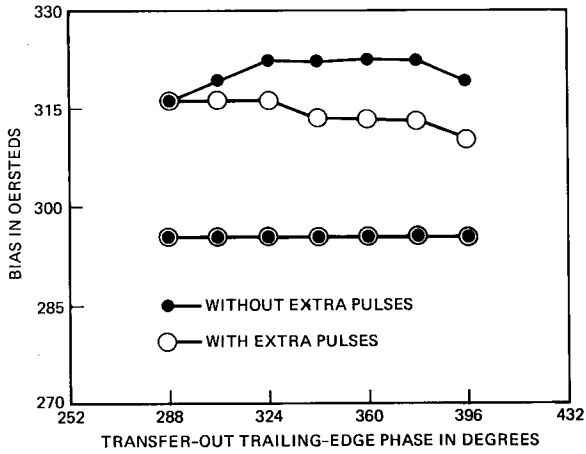

Fig. 19—Bias range vs. transfer-out trailing-edge phase at 55 Oe. The leading-edge phase was 180° and the current was 45 mA.

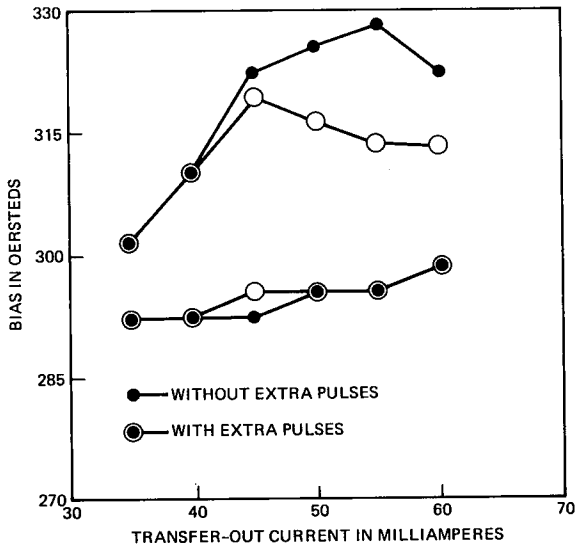

Fig. 20—Bias range vs. transfer-out current at 55 Oe with pulse active from 180° to 306°.

eration. The wide minor-loop margins indicate that low end failure due to stripping or hopping between loops is not the limiting problem at 55 Oe. However, Fig. 3 shows that the low bias limit for minor-loop propagation would increase if the drive could be decreased. Transfer-out limited the overall range at high bias. Figure 20 shows that the high end loss in transfer-out limited is due to interference with bubbles

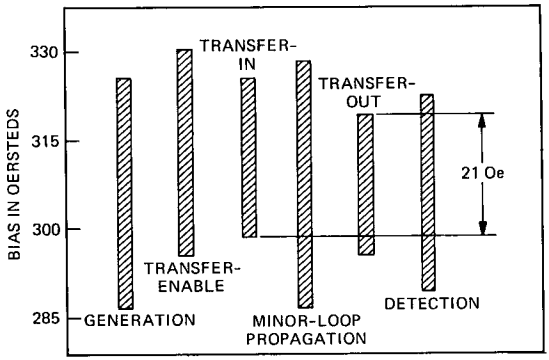

Fig. 21—Bias range for test components at 55 Oe. The generator pulse was 105 mA and 80 ns wide and occurred at 0°. Transfer-enable lasted from −72° to +36° at 35 mA. Transfer-in was 35 mA from 0° to 144°. Transfer-out was 45 mA from 180° to 306°.

in adjacent minor-loop positions. The next limit at high bias was due to detection. The low bias limit was caused by transfer-in. Since the low bias limit increases with increasing transfer-in current, some sort of stripping is indicated. The low drive limit, 50 Oe, was caused by bubbles sticking in the cusps of the clover-leaf-shaped major path features.

In summary, an experimental 4-μm-period functional major-minor bubble device has been operated at 55-Oe drive with 21-Oe bias range. Generation and detection were demonstrated to have a good bias range down to 44-Oe drive, and good minor-loop propagation was obtained as low as 33 Oe.

VII. ACKNOWLEDGMENTS

It is a pleasure to thank A. J. Perneski, S. L. Blank, P. I. Bonyhard, J. E. Geusic, and C. J. Mogab for helpful comments and suggestions. We also thank our colleagues R. C. LeCraw, R. D. Pierce, and J. F. Dillon, Jr. for various measurements during the course of this work. H. C. Alder provided expert technical assistance.

REFERENCES

1. M. H. Kryder, "Magnetic Bubble Device Scaling and Density Limits," IEEE Trans. Magn., *MAG-15,* No. 3 (May 1979), pp. 1009–16.
2. R. E. Fontanta, Jr., D. C. Bullock, and S. K. Singh, "Characteristics of a 1Mbit/1 cm^2 Magnetic Bubble Memory," IEEE Trans. Magn., *MAG-16,* No. 5 (September 1980), pp. 1101–5.
3. T. Yanase, S. Orihara, and K. Yamagishi, "Design Consideration for a 4 μm Period Permalloy Bubble Device," Paper No. DB-01, 3rd Joint Intermag-MMM Conference, Montreal, Canada, 20–23 July 1982.
4. Y. S. Lin et al., "Self-Aligned Contiguous Disk Chip Using 1 μm Bubbles and Charged-Wall Functions," IEEE Trans. Magn., *MAG-15,* No. 6 (November 1979), pp. 1642–7.

5. R. Wolfe et al., "Ion-Implanted Patterns for Magnetic Bubble Propagation," AIP Conf. Proc., *10* (November 1972), pp. 339–43.
6. K. Komenou et al., "Development of an Ion Implanted Bubble Device with 4 μm Period," IEEE Trans. Magn., *MAG-17* (November 1981), pp. 2908–13.
7. S. L. Blank et al., "Design and Development of Single-Layer, Ion-Implantable Small Bubble Materials for Magnetic Bubble Devices," J. Appl. Phys., *50,* No. 3, Part II (March 1979), pp. 2155–60.
8. R. C. LeCraw et al., "Effect of Lanthanum on Growth-Induced Anisotropy in LPE Bubble Garnet Films," IEEE Trans. Magn., *MAG-13,* No. 5 (September 1977), pp. 1092–4.
9. G. P. Vella-Coleiro, "Measurement of Magnetostriction Coefficients of Epitaxial Garnet Films," Rev. Sci. Instrum., *50,* No. 9 (September 1979), pp. 1130–2.
10. J. G. Skinner, "Life with EBES," Kodak Microelectronics Seminar Proceedings, Interface '76 (October 1976), pp. 92–9.
11. J. M. Moran and D. Maydan, "High Resolution, Steep Profile Resist Patterns," B.S.T.J. *58,* No. 5 (May–June 1979), pp. 1027–36.
12. T. J. Nelson et al., "Design of Bubble Device Elements Employing Ion-Implanted Propagation Elements," B.S.T.J., *59,* No. 2 (February 1980), pp. 229–57.
13. T. J. Nelson et al., "Ion-Implanted Bubble Circuit Function Design," IEEE Trans. Magn. *MAG-17,* No. 1 (January 1981), pp. 1134–41.

AUTHORS

Dirk J. Muehlner, A.B. (Physics), 1965, University of California at Berkeley; Ph.D. (Physics), 1970, Massachusetts Institute of Technology; Instructor and Assistant Professor (Physics), M.I.T., 1970–1979; AT&T Bell Laboratories, 1979—. At M.I.T. Mr. Muehlner worked first on far infrared studies of cosmic background radiation and later on infrared nonlinear optics. Since joining AT&T Bell Laboratories he has worked on high-density magnetic bubble memories.

Terence J. Nelson, B.S. (Electrical Engineering), 1961, Iowa State University; M.E.E., 1963, New York University; AT&T Bell Laboratories, 1961–1963; Ph.D. (Physics), 1967, Iowa State University; AEC Postdoctoral Fellow, 1967–1969, Iowa State University and Lawrence Radiation Laboratory, Berkeley, California; AT&T Bell Laboratories, 1969—. During his first stay at AT&T Bell Laboratories, Mr. Nelson worked on ultrasonic delay lines and digital light deflection. In his doctoral and postdoctoral work, he specialized in mathematical physics, especially relativistic wave equations. He is coauthor of a graduate textbook on electric and magnetic fields. When he returned to AT&T Bell Laboratories, Mr. Nelson studied mode locking in lasers, and later he became involved with magnetic bubble device development. His interests in bubble technology have included bubble nucleation, single-level devices, optimized chevron detectors, and bubble devices based on ion-implanted propagation patterns. Member, Eta Kappa Nu, Sigma Xi, Phi Kappa Phi, American Physical Society.

Virendra V. S. Rana, B. Tech, 1967 (Metallurgical Engineering), Indian Institute of Technology, Kharagpur; M.S., 1971 (Materials Science), State University of New York, Stony Brook; Ph.D., 1977 (Materials Science), University of Southern California, Los Angeles; AT&T Bell Laboratories, 1979—. Before joining AT&T Bell Laboratories, Mr. Rana worked as a Research Scientist in the Materials Science Department at the University of Southern California. His research interests included work in the fracture of materials, liquid-phase sintering of ceramics, and investigation of defects in compound semiconductors. At AT&T Bell Laboratories he has been involved with developing new materials for magnetic bubble devices and investigating

the crystal growth aspects of the liquid-phase epitaxial technique. Currently, he is working on processes and technology for producing silicon integrated circuits.

Bernard J. Roman, B.S. (Physics), 1962, Carnegie-Mellon University; Ph.D. (Physics), Northwestern University, Evanston, Illinois; AT&T Bell Laboratories, 1969—. At AT&T Bell Laboratories, Mr. Roman has been responsible for the development of many processing techniques related to magnetic bubble device fabrication and for the successful transfer of these techniques into manufacture at AT&T Technologies, Inc. His current interests include the investigation of various high-density, fine-line lithography approaches to magnetic bubble fabrication.

George P. Vella-Coleiro, B.Sc. (Science), 1961, Royal University of Malta; M.A. (Physics), 1963, Ph.D. (Physics), 1967, Oxford University; AT&T Bell Laboratories, 1967—. At AT&T Bell Laboratories, Mr. Vella-Coleiro has been investigating the fundamental properties of magnetic bubble materials. Rhodes Scholar, 1961–64; Member, American Physical Society, IEEE.